JACS
JOURNAL OF THE AMERICAN CHEMICAL SOCIETY

Open Access
This article is licensed under CC-BY 4.0

pubs.acs.org/JACS
Communication

Overall Water Splitting by a $SrTaO_2N$-Based Photocatalyst Decorated with an Ir-Promoted Ru-Based Cocatalyst

Kaihong Chen,[#] Jiadong Xiao,[#] Junie Jhon M. Vequizo, Takashi Hisatomi, Yiwen Ma, Mamiko Nakabayashi, Tsuyoshi Takata, Akira Yamakata, Naoya Shibata, and Kazunari Domen*

Cite This: J. Am. Chem. Soc. 2023, 145, 3839−3843

Read Online

ACCESS | Metrics & More | Article Recommendations | Supporting Information

ABSTRACT: The development of narrow-bandgap photocatalysts for one-step-excitation overall water splitting (OWS) remains a critical challenge in the field of solar hydrogen production. $SrTaO_2N$ is a photocatalytic material having a band structure suitable for OWS under visible light ($\lambda \leq 600$ nm). However, the presence of defects in the oxynitride and the lack of cocatalysts to promote simultaneous hydrogen and oxygen evolution make it challenging to realize OWS using this material. The present work demonstrates a $SrTaO_2N$-based particulate photocatalyst for OWS. This photocatalyst, which was composed of single crystals, was obtained by nitriding $SrCl_2$ and Ta_2O_5 together with NaOH, with the latter added to control the formation of defects. The subsequent loading of bimetallic $RuIrO_x$ nanoparticles accelerated charge separation and allowed the $SrTaO_2N$ photocatalyst to exhibit superior OWS activity. This research presenting the strategies of controlling the oxygen sources and promoting the cocatalyst function is expected to expand the range of potential OWS-active oxynitride photocatalysts and permit the design of efficient cocatalysts for photocatalytic OWS.

Downloaded via 64.49.39.237 on July 21, 2026 at 23:19:26 (UTC).
See https://pubs.acs.org/sharingguidelines for options on how to legitimately share published articles.

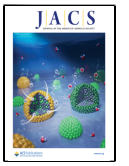
One-step-excitation overall water splitting (OWS) using sunlight and a particulate photocatalyst offers a simple route to the realization of sustainable hydrogen production.[1,2] Recently, solar hydrogen production on the 100 m^2 scale has been achieved based on OWS with an Al-doped $SrTiO_3$ particulate photocatalyst, thus demonstrating the feasibility of this process on a large scale.[3] Nevertheless, the solar-to-hydrogen (STH) energy conversion efficiency of this 100 m^2 panel system was only approximately 0.76%.[3] In fact, increasing the STH efficiency of such systems beyond 1.7% is considered impossible because the photocatalyst responds solely to ultraviolet light.[1] Obtaining an STH efficiency of 5%, which is the lowest value at which this process becomes practical, will require the development of the OWS photocatalysts having band gap energies, E_g, below 2.1 eV.[1] To date, InGaN-based nanorod arrays directly grown on a substrate have demonstrated STH of 3−5%.[4,5] However, only a few particulate photocatalysts, such as $LaMg_{1/3}Ta_{2/3}O_2N$,[6,7] Ta_3N_5,[8] $Y_2Ti_2O_5S_2$,[9] and $BaTaO_2N$,[10] have been reported to have $E_g \leq 2.1$ eV and to drive OWS, and the apparent quantum yield (AQY) under visible light was at most 0.36%.[9]

$SrTaO_2N$ (E_g = 2.1 eV) is a perovskite-type oxynitride photocatalyst with a band structure suitable for promoting both the hydrogen evolution reaction (HER) and oxygen evolution reaction (OER) from aqueous solutions under visible light. To date, $SrTaO_2N$ has been applied to drive either the HER or OER individually in the presence of sacrificial reagents[11,12] but has not been successfully applied to OWS. This is partly due to the inevitable presence of defects in $SrTaO_2N$ that enhance charge recombination. Another crucial factor is the lack of cocatalysts to promote charge separation and simultaneous HER and OER. The dual cocatalyst strategy in which both a hydrogen evolution cocatalyst (HEC) and oxygen evolution cocatalyst (OEC) are incorporated into the OWS system has become popularly investigated to promote OWS effectively.[10,13,14] However, the possible HEC candidates are presently limited to certain noble metals.[2] Bimetals and bimetallic oxides may provide enhanced activities compared with monometallic cocatalysts owing to the tunability of physicochemical properties.[15,16] Therefore, it would be desirable to explore the design of simple yet effective methods for synthesizing $SrTaO_2N$ with few defects and loading bimetallic metal or metal-oxide nanoparticles on photocatalyst surfaces jointly.

The present work demonstrates the application of a $SrTaO_2N$-based particulate photocatalyst to promote OWS. The direct nitridation of $SrCl_2$ and Ta_2O_5 in the presence of NaOH produced single-crystal $SrTaO_2N$ particles with few defects and byproducts. Loading nanoparticles of the bimetallic $RuIrO_x$ with the CrO_y shell on this material allowed the $SrTaO_2N$ photocatalyst to exhibit superior OWS activity compared with other perovskite oxynitride photocatalysts.

$SrTaO_2N$ was synthesized by the nitridation of $SrCl_2$, Ta_2O_5, and NaOH combined in a 4:1:n molar ratio. Here, the $SrCl_2$ served as the Sr source as well as the flux, while the NaOH served as the O source and the flux. This material is referred to herein as $SrTaO_2N(n)$, where n is the NaOH/Ta_2O_5 molar ratio.

Received: October 18, 2022
Published: January 20, 2023



ACS Publications
© 2023 The Authors. Published by American Chemical Society

https://doi.org/10.1021/jacs.2c11025
J. Am. Chem. Soc. 2023, 145, 3839−3843

The X-ray diffraction (XRD) patterns in Figure 1A indicate that a combination of $SrTaO_2N$ and Ta_3N_5 phases was formed

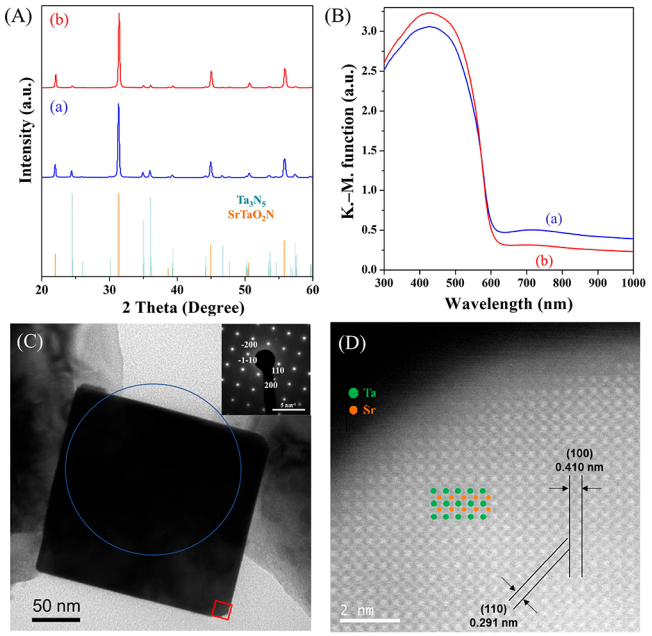


Figure 1. (A) XRD patterns and (B) DRS spectra for (a) $SrTaO_2N(0)$ and (b) $SrTaO_2N(1)$. (C) TEM with SAED and (D) ADF-STEM of a cross-section of the $SrTaO_2N(1)$ sample. The blue circle and red square indicate the areas assessed by SAED and ADF-STEM, respectively.

in the case of $SrTaO_2N(0)$. The amount of Ta_3N_5 in the product was decreased when adding NaOH during the synthesis of the $SrTaO_2N(1)$ specimen. Additional characterization by inductively coupled plasma-atomic emission spectroscopy (ICP-AES) and X-ray photoelectron spectroscopy (XPS) indicated that $SrTaO_2N(1)$ was not doped with Na (Figure S1a). The weight fractions of Sr, Ta, O, and N were measured to be 23.0, 61.1, 5.3, and 8.5%, respectively, indicating that the sample consisted of $0.78(SrTaO_2N) + 0.07(Ta_3N_5)$. The data acquired using UV−visible diffuse-reflectance spectroscopy (DRS) as presented in Figure 1B and Figure S2B demonstrate that the optical absorption edge for each $SrTaO_2N(n)$ sample was at approximately 600 nm regardless of the value of n. An absorption background associated with defects in the photocatalyst is also observed beyond the absorption edge. Notably, these features related to defects and byproducts became weaker with an increasing amount of NaOH, and pure $SrTaO_2N$ was obtained at $n = 2$ (Figure S2). These results suggest that adding appropriate amounts of NaOH can reduce the defect density of $SrTaO_2N$ and the amount of the Ta_3N_5 byproduct.

The selected area electron diffraction (SAED) pattern and the matching of the lattice spacings of $SrTaO_2N(1)$ with those of a reference $SrTaO_2N$ crystal structure[12] suggest the formation of single-crystal $SrTaO_2N$ nanoparticles (Figures 1C and D). The average size of the cube-like $SrTaO_2N(1)$ particles was determined to be 124 nm (Figures S1b and S1c). Rod-like particles were also observed in high-resolution transmission electron microscopy (HR-TEM) images. These particles were found not to include Sr species based on analyses by energy dispersive X-ray spectroscopy (EDS) and therefore attributed to Ta_3N_5 (Figure S3).

$SrTaO_2N(1)$ sequentially loaded with IrO_2 by microwave-assisted heating (denoted as $IrO_{2(MW)}$), Ru by impregnation-H_2 reduction, and CrO_y by photodeposition (see the Supporting Information for details) were capable of evolving H_2 and O_2 from water simultaneously under visible light ($\lambda >$ 420 nm) with initial evolution rates of 9.1 and 3.0 μmol h^{-1}, respectively (Figure 2A). The deviation from the stoichio-

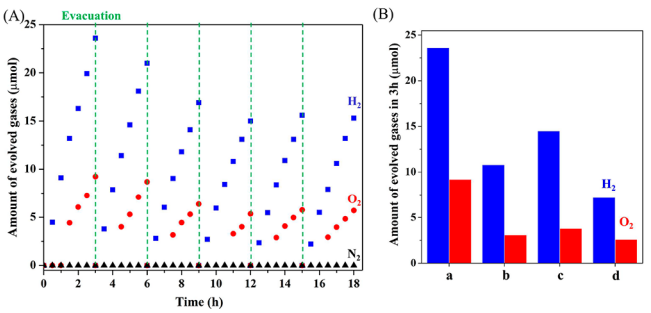


Figure 2. (A) Gas evolution over time using $CrO_y/Ru/IrO_{2(MW)}/SrTaO_2N(1)$ in water under visible light ($\lambda >$ 420 nm). (B) Amounts of gas products during the 3-h OWS reaction using $SrTaO_2N(1)$ modified with different cocatalysts: (a) $CrO_y/Ru/IrO_{2(MW)}$, (b) CrO_y/Ru, (c) $CrO_y/Ru/IrO_{2(AD)}$, and (d) $IrO_{2(AD)}/CrO_y/Ru$.

metric ratio of the two was due to low quantification accuracy near the detection limit of O_2 (Figure S4A). The optimal nominal Ir, Ru, and Cr contents were 1, 4, and 4 wt %, respectively (Table S1), while the actual loading proportions were found to be 0.8, 4.0, and 0.6 wt %, respectively, by ICP-AES. The AQY in response to irradiation at 420 ± 30 nm was determined to be 0.34% in the initial stage of the reaction. A slight loss in the OWS activity was observed after three repeated uses of the photocatalyst, after which the performance remained essentially constant with further use. The STH value was measured to be 5−6 × 10^{-3}% over the 48-h reaction (Figure S4B). $SrTaO_2N(0)$ prepared in the absence of NaOH exhibited lower OWS activity because of higher defect density and impurity Ta_3N_5 content (Figure S2C). On the other hand, $SrTaO_2N(2)$ prepared with a larger NaOH amount also exhibited lower OWS activity even though it comprised single-phase $SrTaO_2N$. Notably, single-phase $SrTaO_2N$ was also obtained by using $SrCO_3$ instead of NaOH (Figure S5), but it could not split water in this study. These results suggest the importance of controlling the amount of oxygen sources to produce stoichiometric and active $SrTaO_2N$. The optimal $NaOH/Ta_2O_5$ molar ratio in the original formulation was unity.

The cocatalysts evidently had a significant effect on the OWS activity. The OWS activity decreased without the loading of $IrO_{2(MW)}$ (Figure 2B). Adsorption of colloidal IrO_2 (denoted as $IrO_{2(AD)}$) before or after the loading of the CrO_y/Ru cocatalyst was not effective in enhancing OWS although $IrO_{2(AD)}$ effectively promoted the reaction on $Y_2Ti_2O_5S_2$,[9] $BaTaO_2N$,[10] and TaON.[14] Therefore, an in-depth understanding of the structures and functions of the $CrO_y/Ru/IrO_{2(MW)}$ cocatalyst is imperative.

The annular dark-field scanning TEM (ADF-STEM) images of the $CrO_y/Ru/IrO_{2(MW)}/SrTaO_2N(1)$ specimen in Figure 3 indicate that the Ru particle size in the present samples was around 5 nm. The EDS images show that typical core (Ru species)-shell (Cr species) nanostructures were obtained. The CrO_y shell capping the noble metal is essential to suppress the

https://doi.org/10.1021/jacs.2c11025
J. Am. Chem. Soc. 2023, 145, 3839−3843

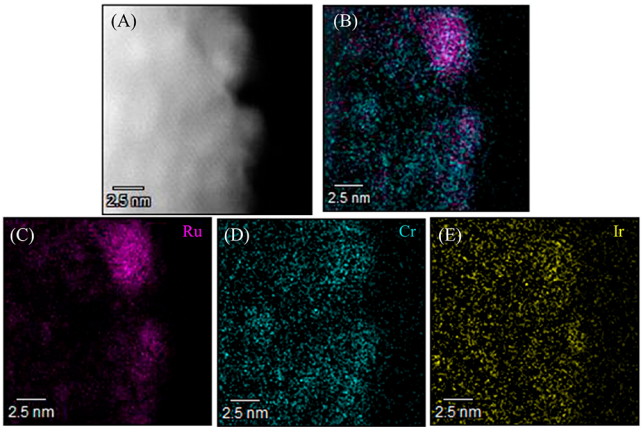


Figure 3. (A) ADF-STEM images and (B-E) STEM-EDS elemental maps of the CrO_y/Ru/$IrO_{2(MW)}$/$SrTaO_2N(1)$ specimen. (B) Superimposition of Ru and Cr, (C) Ru, (D) Cr, and (E) Ir.

reverse reaction during the OWS.[8−10] The XRD pattern for the Ru/$IrO_{2(MW)}$/$SrTaO_2N(1)$ suggests the copresence of metallic Ru and RuO_2 (Figure S6). The latter compound likely resulted from surface oxidation of Ru^0 nanoparticles, in agreement with our previous results.[14] On the other hand, the Ir species showed weak signals distributed over the entire $SrTaO_2N(1)$ particles in STEM-EDS analysis, and their structure was unclear.

To gain the information about the chemical states, the Ir species loaded on $SrTaO_2N(1)$ was analyzed by XPS (Figure 4A). The Ir species in $IrO_{2(MW)}$/$SrTaO_2N(1)$ was attributed to

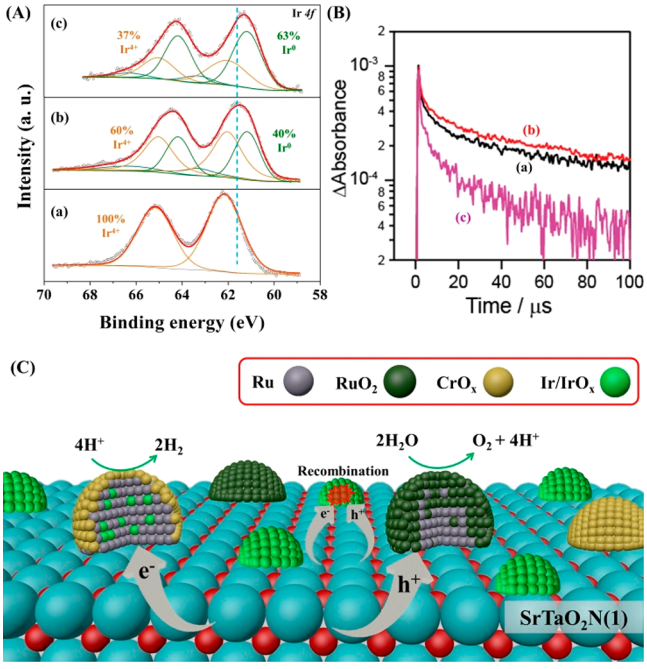


Figure 4. (A) Deconvoluted Ir 4*f* XPS spectra for $SrTaO_2N(1)$ specimens loaded with (a) $IrO_{2(MW)}$, (b) $IrO_{2(MW)}$ and reduced without loading Ru, and (c) Ru/$IrO_{2(MW)}$. (B) Transient decay profiles of photogenerated electrons probed at 5000 nm of $SrTaO_2N(1)$ specimens (a) without cocatalysts and loaded with (b) Ru and (c) Ru/$IrO_{2(MW)}$. (C) An illustration showing the structure and dispersion of cocatalysts on the photocatalyst surface together with the dominant charge transfer processes.

IrO_2 on the basis of the Ir $4f_{7/2}$ and $4f_{5/2}$ signals at binding energies of 62.2 and 65.2 eV, respectively.[17] After the H_2 reduction, the Ir peaks shifted to lower binding energies, indicative of partial reduction to metallic Ir. The fraction of metallic Ir became greater in the presence of Ru to produce the Ru/$IrO_{2(MW)}$ cocatalyst. Concurrently, the fraction of metallic Ru was decreased by the presence of $IrO_{2(MW)}$ compared with the sample without Ir, as shown in the Ru 3*p* XPS analysis (Figure S7). The opposite movements of the Ir and Ru peaks suggest that there were certain electronic interactions between them in the Ru/$IrO_{2(MW)}$ cocatalyst owing to the formation of the RuIr bimetal and $RuIrO_2$ bimetallic oxide nanoparticles (denoted as $RuIrO_x$ for simplicity).[18] Taking the additional EDS mapping results (Figure S8) into account, it can be concluded that RuO_x, $RuIrO_x$, and IrO_x nanoparticles were primarily present on the $SrTaO_2N(1)$ surface.

The roles of IrO_x, RuO_x, and $RuIrO_x$ cocatalysts during photocatalytic OWS were further assessed by transient absorption spectroscopy (TAS) (Figure S9).[19] Probing at a wavelength of 5000 nm (~0.25 eV) upon band gap excitation of $SrTaO_2N(1)$ by a 470 nm pump was used to monitor the decay behavior of electrons (Figure 4B). When only RuO_x was loaded on $SrTaO_2N(1)$ (i.e., Ru/$SrTaO_2N(1)$), the intensity of the absorption at 5000 nm increased, and the decay was notably slower compared with that observed for bare $SrTaO_2N(1)$. These data demonstrate that Ru/RuO_x served not only as an HEC but also as an OEC and captured photogenerated holes in $SrTaO_2N(1)$. These outcomes agree with the observed promotion of the sacrificial HER and OER activities upon loading Ru onto $SrTaO_2N(1)$ (Figure S10). When Ir was included in RuO_x (i.e., Ru/$IrO_{2\ (MW)}$/$SrTaO_2N$-(1)) to form the new cocatalyst $RuIrO_x$, the decay of electrons in $SrTaO_2N(1)$ was greatly accelerated. Considering the notable enhancement in the sacrificial HER and OER activities compared with the Ru/$SrTaO_2N(1)$ specimen (Figure S10), this implies that $RuIrO_x$ captured electrons very efficiently from $SrTaO_2N$ and worked as an active HEC. Moreover, the TAS results (Figure S11) for $IrO_{2(MW)}$/$SrTaO_2N(1)$ subjected to the reduction treatment indicate both electrons and holes could be captured by IrO_x, leading to enhanced charge recombination. Collectively, $RuIrO_x$, having significant electron capture capacity, with a CrO_y shell worked as an active HEC, while RuO_x served as a passable OEC (Figure 4C). The IrO_x species present in minor amounts most likely formed recombination centers that were detrimental to the OWS.

In summary, this work established a $SrTaO_2N$-based one-step-excitation OWS system. By reducing the defect density in $SrTaO_2N$ based on adding NaOH and by the formation of $RuIrO_x$ cocatalysts that promoted charge separation and surface reactions, this OWS system achieved an STH value of 6.3×10^{-3}% and an AQY (420 ± 30 nm) of 0.34%. These are one of the highest values yet reported for a perovskite oxynitride photocatalyst with $E_g \leq 2.1$ eV. $RuIrO_x$ and RuO_x were found to work as an HEC and OEC, respectively. Further activity improvements are expected by controlling the morphology of the photocatalyst particles to make facet-selective deposition of these cocatalysts feasible.[20] Controlling the oxygen source during the nitridation and promoting the cocatalyst function by forming bimetallic systems will help the development of other semiconductor/cocatalyst systems for OWS.

https://doi.org/10.1021/jacs.2c11025
J. Am. Chem. Soc. 2023, 145, 3839−3843

■ ASSOCIATED CONTENT

Supporting Information

The Supporting Information is available free of charge at https://pubs.acs.org/doi/10.1021/jacs.2c11025.

Experimental details; additional characterization and reaction results (PDF)

■ AUTHOR INFORMATION

Corresponding Author

Kazunari Domen − *Research Initiative for Supra-Materials, Interdisciplinary Cluster for Cutting Edge Research, Shinshu University, Nagano 380-8553, Japan; Office of University Professors, The University of Tokyo, Tokyo 113-8656, Japan;* orcid.org/0000-0001-7995-4832; Email: domen@shinshu-u.ac.jp

Authors

Kaihong Chen − *Research Initiative for Supra-Materials, Interdisciplinary Cluster for Cutting Edge Research, Shinshu University, Nagano 380-8553, Japan;* orcid.org/0000-0002-7513-0892

Jiadong Xiao − *Research Initiative for Supra-Materials, Interdisciplinary Cluster for Cutting Edge Research, Shinshu University, Nagano 380-8553, Japan;* orcid.org/0000-0001-9130-5376

Junie Jhon M. Vequizo − *Research Initiative for Supra-Materials, Interdisciplinary Cluster for Cutting Edge Research, Shinshu University, Nagano 380-8553, Japan;* orcid.org/0000-0003-2490-2335

Takashi Hisatomi − *Research Initiative for Supra-Materials, Interdisciplinary Cluster for Cutting Edge Research, Shinshu University, Nagano 380-8553, Japan; PRESTO, JST, Nagano 380-8553, Japan;* orcid.org/0000-0002-5009-2383

Yiwen Ma − *Research Initiative for Supra-Materials, Interdisciplinary Cluster for Cutting Edge Research, Shinshu University, Nagano 380-8553, Japan*

Mamiko Nakabayashi − *Institute of Engineering Innovation, The University of Tokyo, Tokyo 113-8656, Japan*

Tsuyoshi Takata − *Research Initiative for Supra-Materials, Interdisciplinary Cluster for Cutting Edge Research, Shinshu University, Nagano 380-8553, Japan*

Akira Yamakata − *Graduate School of Natural Science & Technology, Okayama University, Okayama 700-8530, Japan;* orcid.org/0000-0003-3179-7588

Naoya Shibata − *Institute of Engineering Innovation, The University of Tokyo, Tokyo 113-8656, Japan;* orcid.org/0000-0003-3548-5952

Complete contact information is available at: https://pubs.acs.org/10.1021/jacs.2c11025

Author Contributions

#K.C. and J.X. contributed equally to this work.

Notes

The authors declare no competing financial interest.

■ ACKNOWLEDGMENTS

This work was financially supported by the Artificial Photosynthesis Project of the New Energy and Industrial Technology Development Organization (NEDO) and JST-PRESTO (grant no. JPMJPR20T9). Part of this work was conducted at the Advanced Characterization Nanotechnology Platform of the University of Tokyo, supported by the "Nanotechnology Platform" of the Ministry of Education, Culture, Sports, Science and Technology (MEXT), Japan (grant no. JPMXP09-A-22-UT-0023). K.C. acknowledges support from the Japanese Society for Promotion of Sciences (JSPS) for Overseas Researchers and the National Natural Science Foundation of China (grant no. 22005154). The authors also thank Ms. Michiko Obata (Shinshu University) and Ms. Keiko Kato (University of Tokyo) for their assistance in performing XPS and elemental analyses, respectively.

■ REFERENCES

(1) Hisatomi, T.; Domen, K. Reaction systems for solar hydrogen production via water splitting with particulate semiconductor photocatalysts. *Nat. Catal.* **2019**, *2*, 387−399.

(2) Tao, X. P.; Zhao, Y.; Wang, S. Y.; Li, C.; Li, R. G. Recent advances and perspectives for solar-driven water splitting using particulate photocatalysts. *Chem. Soc. Rev.* **2022**, *51*, 3561−3608.

(3) Nishiyama, H.; Yamada, T.; Nakabayashi, M.; Maehara, Y.; Yamaguchi, M.; Kuromiya, Y.; Nagatsuma, Y.; Tokudome, H.; Akiyama, S.; Watanabe, T.; Narushima, R.; Okunaka, S.; Shibata, N.; Takata, T.; Hisatomi, T.; Domen, K. Photocatalytic solar hydrogen production from water on a 100-m^2 scale. *Nature* **2021**, *598*, 304−307.

(4) Chowdhury, F. A.; Trudeau, M. L.; Guo, H.; Mi, Z. A photochemical diode artificial photosynthesis system for unassisted high efficiency overall pure water splitting. *Nat. Commun.* **2018**, *9*, 1707.

(5) Wang, Y.; Wu, Y.; Sun, K.; Mi, Z. A quadruple-band metal-nitride nanowire artificial photosynthesis system for high efficiency photocatalytic overall solar water splitting. *Mater. Horizons* **2019**, *6*, 1454−1462.

(6) Pan, C. S.; Takata, T.; Nakabayashi, M.; Matsumoto, T.; Shibata, N.; Ikuhara, Y.; Domen, K. A complex perovskite-type oxynitride: The first photocatalyst for water splitting operable at up to 600 nm. *Angew. Chem., Int. Ed.* **2015**, *54*, 2955−2959.

(7) Pan, C.; Takata, T.; Domen, K. Overall Water splitting on the transition-metal oxynitride photocatalyst $LaMg_{1/3}Ta_{2/3}O_2N$ over a large portion of the visible-light spectrum. *Chem. - Eur. J.* **2016**, *22*, 1854−1862.

(8) Wang, Z.; Inoue, Y.; Hisatomi, T.; Ishikawa, R.; Wang, Q.; Takata, T.; Chen, S. S.; Shibata, N.; Ikuhara, Y.; Domen, K. Overall water splitting by Ta_3N_5 nanorod single crystals grown on the edges of $KTaO_3$ particles. *Nat. Catal.* **2018**, *1*, 756−763.

(9) Wang, Q.; Nakabayashi, M.; Hisatomi, T.; Sun, S.; Akiyama, S.; Wang, Z.; Pan, Z. H.; Xiao, X.; Watanabe, T.; Yamada, T.; Shibata, N.; Takata, T.; Domen, K. Oxysulfide photocatalyst for visible-light-driven overall water splitting. *Nat. Mater.* **2019**, *18*, 827−832.

(10) Li, H. H.; Xiao, J. D.; Vequizo, J. J. M.; Hisatomi, T.; Nakabayashi, M.; Pan, Z. H.; Shibata, N.; Yamakata, A.; Takata, T.; Domen, K. One-step excitation overall water splitting over a modified Mg-doped $BaTaO_2N$ photocatalyst. *ACS Catal.* **2022**, *12*, 10179−10185.

(11) Fu, J.; Skrabalak, S. E. Enhanced photoactivity from single-crystalline $SrTaO_2N$ nanoplates synthesized by topotactic nitridation. *Angew. Chem., Int. Ed.* **2017**, *56*, 14169−14173.

(12) Fang, T.; Huang, H. T.; Feng, J. Y.; Hu, Y. F.; Qian, Q. F.; Yan, S. C.; Yu, Z. T.; Li, Z. S.; Zou, Z. G. Reactive inorganic vapor deposition of perovskite oxynitride films for solar energy conversion. *Research* **2019**, *2019*, 9282674.

(13) Maeda, K.; Xiong, A. K.; Yoshinaga, T.; Ikeda, T.; Sakamoto, N.; Hisatomi, T.; Takashima, M.; Lu, D. L.; Kanehara, M.; Setoyama, T.; Teranishi, T.; Domen, K. Photocatalytic overall water splitting promoted by two different cocatalysts for hydrogen and oxygen evolution under visible light. *Angew. Chem., Int. Ed.* **2010**, *49*, 4096−4099.

(14) Xiao, J. D.; Nishimae, S.; Vequizo, J. J. M.; Nakabayashi, M.; Hisatomi, T.; Li, H. H.; Lin, L. H.; Shibata, N.; Yamakata, A.; Inoue,

Y.; Domen, K. Enhanced overall water splitting by a zirconium-doped TaON-based photocatalyst. *Angew. Chem., Int. Ed.* **2022**, *61*, No. e202116573.
(15) Zhou, M.; Li, C.; Fang, J. Noble-metal based random alloy and intermetallic nanocrystals: Syntheses and applications. *Chem. Rev.* **2021**, *121*, 736−795.
(16) Pelicano, C. M.; Saruyama, M.; Takahata, R.; Sato, R.; Kitahama, Y.; Matsuzaki, H.; Yamada, T.; Hisatomi, T.; Domen, K.; Teranishi, T. Bimetallic synergy in ultrafine cocatalyst alloy nanoparticles for efficient photocatalytic water splitting. *Adv. Funct. Mater.* **2022**, *32*, 2202987.
(17) Freakley, S. J.; Ruiz-Esquius, J.; Morgan, D. J. The X-ray photoelectron spectra of Ir, IrO_2 and $IrCl_3$ revisited. *Surf. Interface Anal.* **2017**, *49*, 794−799.
(18) Li, G. Q.; Li, S. T.; Ge, J. J.; Liu, C. P.; Xing, W. Discontinuously covered IrO_2-RuO_2@Ru electrocatalysts for the oxygen evolution reaction: How high activity and long-term durability can be simultaneously realized in the synergistic and hybrid nanostructure. *J. Mater. Chem. A* **2017**, *5*, 17221−17229.
(19) Vequizo, J. J. M.; Hojamberdiev, M.; Teshima, K.; Yamakata, A. Role of CoO_x cocatalyst on Ta_3N_5 photocatalysts studied by transient visible to mid-infrared absorption spectroscopy. *J. Photochem. Photobiol., A* **2018**, *358*, 315−319.
(20) Takata, T.; Jiang, J. Z.; Sakata, Y.; Nakabayashi, M.; Shibata, N.; Nandal, V.; Seki, K.; Hisatomi, T.; Domen, K. Photocatalytic water splitting with a quantum efficiency of almost unity. *Nature* **2020**, *581*, 411−414.

Recommended by ACS

Photocatalytic Overall Water Splitting by $SrTiO_3$: Progress Report and Design Strategies
Celal Avcıolu, Aleksander Gurlo, *et al.*
JANUARY 27, 2023
ACS APPLIED ENERGY MATERIALS
READ

Narrow-Band-Gap Particulate Photocatalysts for One-Step-Excitation Overall Water Splitting
Jiadong Xiao, Kazunari Domen, *et al.*
MARCH 14, 2023
ACCOUNTS OF CHEMICAL RESEARCH
READ

Porous Cuboidal $SrNbO_2N$ Crystals Grown on a Nb Substrate as an Active Photoanode for Neutral Seawater Splitting under Sunlight
Van-Huy Trinh and Jeongsuk Seo
JANUARY 20, 2023
ACS SUSTAINABLE CHEMISTRY & ENGINEERING
READ

Characterization of Hole States at the Zn-Doped Hematite/Water Interface from *Ab Initio* Simulations
Zachary K. Goldsmith, Annabella Selloni, *et al.*
APRIL 04, 2023
ACS CATALYSIS
READ

Get More Suggestions >

https://doi.org/10.1021/jacs.2c11025
J. Am. Chem. Soc. 2023, 145, 3839−3843